Nanoscale

Accepted Manuscript

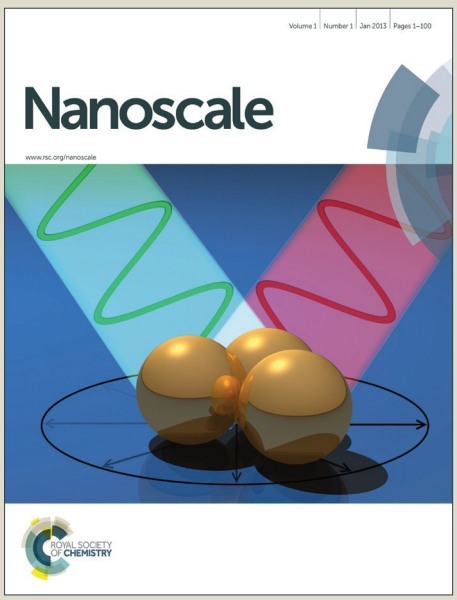

ROYAL SOCIETY OF CHEMISTRY

www.rsc.org/nanoscale

Nanoscale

ARTICLE

Hyperbranched polymer mediated size-controlled synthesis of gadolinium phosphate nanoparticles: colloidal properties and particle size-dependence on MRI relaxivity.

Received 00th January 20xx,
Accepted 00th January 20xx

DOI: 10.1039/x0xx00000x

www.rsc.org/

Camille Frangville[a,‡], Maylis Gallois[a,‡], Yichen Li[b,‡], Hanh Hong Nguyen[a], Nancy Lauth-de Viguerie[a], Daniel R. Talham[b,*], Christophe Mingotaud[a] and Jean-Daniel Marty[a,*]

Abstract: Hyperbranched polymers based on the polyamidoamine, HyPAM, were used to synthesize gadolinium phosphate nanowires under mild conditions. Control of the average particle size was obtained by adjusting polymer concentration. Proton relaxivity measurements reveal an optimum particle size, reaching relaxivity values as high as 55±9 $mM^{-1}.s^{-1}$ for r_1 and 67±11 $mM^{-1}.s^{-1}$ for r_2. The colloidal stability of these hybrid systems were optimized through the use of functionalized core-shell polymers containing PEG segments and C18-PEG segments, structures which also offer the possibility of imparting additional function into the polymer-particle hybrids.

A. Introduction

Magnetic resonance imaging (MRI) is a powerful medical diagnostic tool, the efficiency of which is greatly improved by the use of MRI contrast agents. The two most common classes of contrast agents are[1,2]: (a) T_1 or positive contrast agents that shorten proton longitudinal relaxation time and (b) T_2 or negative contrast agents that shorten proton transversal relaxation time. With seven unpaired electrons and a correspondingly large magnetic moment, molecular complexes of Gd^{3+} are most often employed as T_1 agents.[3,4] On the other hand, superparamagnetic iron oxide nanoparticles (NPs) have seen the most widespread use as T_2 agents.[5,6] There are a number of potential advantages to particle-based agents, including easy surface modification for incorporating specific vectors and the opportunity to combine properties to give multimodal agents.[7,8] Hence, there is interest in developing particle systems that are T_1 agents, and recent reports have described NPs of gadolinium oxides (e.g. Gd_2O_3)[9–12], fluorides (e.g. GdF_3, $NaGdF_4$)[13,14] or phosphates (e.g. $GdPO_4$),[15–21] several of which offer relaxivities per mole of Gd comparable to the common molecular agents. The particles require suitable coatings, such as polymers or organic ligands like dextran[17,18] or DNA,[20] to improve their biocompatibility and reduce their toxicity.

The $GdPO_4$ NPs are of special interest because of the combination of low solubility, ease of surface modification, and the variety of synthetic routes available to form particles.[22] Hydrothermal synthesis[17–19,23,24] and more recently microemulsion synthesis[20] or a templated mineralization process[25] were used to form well-defined $GdPO_4$ NPs as nanorods or nanowires of tens to hundreds nanometers length. Nanoparticles of $GdPO_4$, or even particles with $GdPO_4$ modified-surfaces, have been shown to be compatible with biological media. For example, Li et al. recently demonstrated that pretreatment of rare earth oxide nanoparticles with phosphate protects against *in vivo* biological interference of gadolinium ions with Ca^{2+} involved in cell metabolism as well as pro-fibrogenic effects favored by the presence of Gd^{3+} ions.[26] This result was further supported by cell toxicity and in vivo experimental assays performed with dextran-coated $GdPO_4$NPs that showed no impact on cell viability, observed over long residence times in plasma.[17-18]

Whereas a real interest on the use of $GdPO_4$ NPs exists, chemical recipes to obtain size controlled $GdPO_4$ NPs down to a few nm are still needed. In addition to practical advantages, achieving particle size control with a uniform surface coating will allow precise studies of the size dependence on relaxivity, as has been suggested for Gd_2O_3 NPs although with different surface coatings.[10] To achieve this first objective, hyperbranched polymers are potentially materials of choice. Size controlled gold, silver or platinum NPs have been previously obtained by complexing appropriate precursors within hyperbranched architectures followed by a reduction process.[27–30] To form gadolinium phosphate, a similar strategy can be followed that first sequesters Gd^{3+} within the polymer and then replaces chemical reduction with a precipitation step. For this, we choose here a hyperbranched structure based on the poly(amidoamine) HyPAM possessing amine or amide chemical functions (Scheme 1)[27–29].

Polymers with a HyPAM core functionalized with different shells based on poly(ethyleneglycol) (PEG) were also synthesized (see Scheme 1 and Supplementary Information) to confer stability, biocompatibility[31] and drug-loading capacity to the hybrid NPs. As a novel synthetic route to $GdPO_4$ NPs, the ability of such structures to act as both a growth controlling agent and a stabilizer is investigated in this article. The effect of polymer functionalization

a Laboratoire des Interactions Moléculaires et Réactivités Chimiques et Photochimiques, Université de Toulouse, CNRS UMR 5623, 31062 Toulouse, France.
b Department of Chemistry, University of Florida, Gainesville, Florida 32611-7200, United States
Corresponding Authors: JDM: marty@chimie.ups-tlse.fr, DRT: talham@chem.ufl.edu

Electronic Supplementary Information (ESI) available: NMR spectra and integrations versus gadolinium concentra-tion; TEM pictures and corresponding sizes with size dis-persions for $GdPO_4$/HyPAM and functionalized core-shell hybrids; EDS elemental mapping measurement; relaxation rate plots; DLS correlogram for NaCl addition; Nile Red fluorescence excitation and emission

on both colloidal stability and relaxivity measurements are also presented.

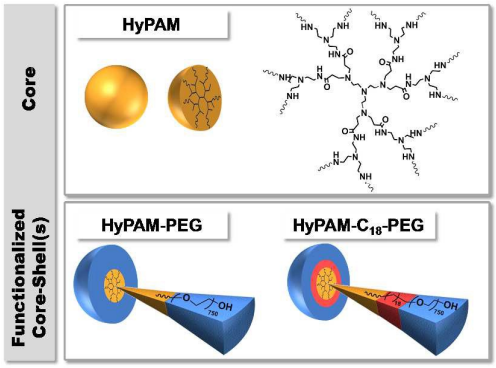

Scheme 1. Hyperbranched polymer structures used for the synthesis of $GdPO_4$ nanoparticles.

B. Experimental Section

B.1. Materials. Gadolinium (III) nitrate hexahydrate, sodium phosphate dibasic, *N*-hydroxysuccinimide, *p*-toluenesulphonic acid, 1,18-octadecanedioic acid, methylacrylate, *N*, *N*'-dicyclohexylcarbodiimide and Nile Red (9-diethylamino-5-benzo-α-phenoxazinone) were purchased from Sigma Aldrich Co. Ltd. at highest purity available (≥99% and ≥98%) and used as received. Tris(2-aminoethyl)amine (Aldrich) was distilled under reduced pressure and stored under argon atmosphere before use. All solvents were purchased from Acros, Fluka or Aldrich and used as received. Water was purified through a filter and ion exchange resin using a Purite device (resistivity 18.2 MΩ·cm). Dialysis was performed with benzoylated 10 FT dialysis tubing from Sigma-aldrich (molecular weight cut-off 2000 g mol^{-1}). For this, a dialysis tube filled with 10 mL $GdPO_4$ solution was dialyzed against 1L of deionized water for 24h at room temperature under stirring. Water was replaced three times.

B.2. Polymer synthesis.

Preparation of hyperbranched polyamidoamine core (HyPAM). The synthesis of the HYPAM cores were carried out following previously published work by our group[27,29,32]. Tris(2-di(methylacrylate)aminoethyl)-amine was first obtained as follows. To 5.3 g of methylacrylate (61.6 mmol) in 6.5 mL of methanol was added dropwise a solution of 1.25 g of freshly distilled tris(2-aminoethyl)amine (8.5 mmol) in 1.5 mL of methanol at 0°C under argon atmosphere. The mixture was then stirred at room temperature for two days. The product (5.9 g) was obtained, after elimination of the solvent under vacuum, as a light yellow oil and used without further purification steps. Then, 2.5 g of tris(2-aminoethyl)amine (17.1 mmol) were mixed with 1.13 g of tris(2-di(methylacrylate)aminoethyl)amine (1.7 mmol). The solution was stirred under argon atmosphere at 75°C during two days, at which time the products were dissolved in 5 mL CH_2Cl_2 and precipitated into 200 mL THF at 0°C. The polymer precipitated as a yellow gum, yielding 2.05 g. HyPAM: ^{1}H NMR (DMSO-d_6, 500 MHz): 2.24 (m, N-*CH*$_2$-*CH*$_2$-N); 2.45 (m, CO-NH-CH$_2$-*CH*$_2$-N); 2.51 (DMSO and m, -*CH*$_2$-NH$_2$); 2.63 (m, N-*CH*$_2$-CH$_2$-CO); 2.7 (m, N-CH$_2$-*CH*$_2$-CO); 3.1 (m, -*CH*$_2$-NH-CO-); 3.45 (NH); ^{13}C NMR (DMSO-d6, 500 MHz): 33.79 (N-*CH*$_2$-*CH*$_2$-N); 37.34 (-*CH*$_2$-NH-CO-); 41.62 (N-CH$_2$-*CH*$_2$-CO); 46.15 (-*CH*$_2$-NH$_2$); 47.43 (N-*CH*$_2$-CH$_2$-CO); 56.61 (CO-NH-CH$_2$-*CH*$_2$-N); 172.0 (*CO*); IR (HyPAM): $\bar{\nu}$ = 3345, 3283, 3078, 2943, 2858, 2824, 1645, 1557, 1460, 1354, 1291, 1096, 1062, 946, 915 cm^{-1}.

Double and single shell synthesis. Used to prepare the double-shell structure, the synthesis of the building block **mPEG$_{750}$-C17-COOH (1)** has been previously described.[33] Briefly, 1 eq. of mPEG$_{750}$-OH, 4 eq. of 1,18-octadecanedioic acid and 2.5 mol% *p*-toluenesulphonic acid (PTSA) in toluene were stirred under reflux in a flask equipped with a Dean-Stark trap for 24 h. The solution was then cooled down to 0 ºC, the excess of diacid was filtered off, and the mixture concentrated by removal of the solvent. Purification was achieved by flash chromatography with a gradient $CHCl_3$:MeOH 10:0 to 10:1 (v:v) as eluent. The single-shell building block **mPEG$_{750}$-COOH (2)** was prepared by oxidation with Jones reagent adapting a procedure published elsewhere. Typically, 20 g of mPEG$_{750}$-OH was dissolved in 200 mL of acetone, 48.6 mL of Jones reagent **(**8.99 g of CrO_3 dissolved in 64.20 mL of water and the solution cooled down to 10 °C. To this, 7.80 mL of concentrated H_2SO_4 were added dropwise under stirring and the mixture was allowed to reach room temperature.) was added and the solution stirred at room temperature over 20 h. The reaction was quenched by addition of 5 mL of isopropanol. The crude product was concentrated and purified by *silica* gel *column* chromatography prepared with a 95:5 (v:v) $CHCl_3$:TEA mixture and using a gradient eluent of $CHCl_3$:MeOH from 99:1 to 90:10 (v:v). A total of 6.41 g of pure mPEG$_{750}$-COOH were recovered (Yield: 34%). ^{1}H NMR (400 MHz, $CDCl_3$) δ: 4.01 (s, O-*CH*$_2$-COOH); 3.80-3.44 (m large, PEG backbone); 3.35 (s, -O-*CH*$_3$); 3.04 (q, Et_3N traces: N(*CH*$_2$-CH$_3$)$_3$); 1.25 (t, Et_3N traces: N(CH$_2$-*CH*$_3$)$_3$). ^{13}C NMR (100 MHz, $CDCl_3$) δ: 174.19 (-O-CH$_2$-*COOH*); 71.86 (-*CH*$_2$-O-CH$_3$); 70.49 (br *PEG*); 70.00 (-O-*CH*$_2$-COOH); 58.95 (-O-*CH*$_3$) ppm.

Grafting of PEG$_{750}$-C$_{17}$-COOH or PEG$_{750}$-COOH onto the HYPAM core. *N*-hydroxysuccinimide (SuOH) (1 eq.) and *N*, *N*'-dicyclohexylcarbodiimide (DCC) (1.05 eq.) were added to 1 eq. of **(1)** or **(2)** in THF. The mixture was stirred at room temperature for 12-20 h and then kept at 50 °C overnight to crystallize 1,3-dicyclohexylurea (DCU). After filtration this procedure was repeated several times until no more DCU visibly crystallized. The solvent was removed *in vacuo* and the obtained shell building blocks and were used without further purification. For coupling, the shell building block (1.05 eq.) was added to the hyperbranched core HyPAM (1 eq. of NH_2 groups) in methanol and stirred for 24 h at room temperature. The resulting core-(multi)shell structures were purified by dialysis in methanol for 3 days with three solvent changes. HYPAM-PEG: ^{1}H NMR (400MHz, D_2O) δ: 3.71 (br, -O-*CH*$_2$-*CH*$_2$-O- from mPEG); 3.34 (s, -O-*CH*$_3$ from mPEG); (3.39 (br, -CO-NH-*CH*$_2$-); 2.79 (br, N-*CH*$_2$-CH$_2$-CO); 2.79 (br, NH$_2$-*CH*$_2$-); 2.67 (br, N-*CH*$_2$-CH$_2$-NH-CO); 2.67 (br, N-CH$_2$-CH$_2$-N-); 2.45 (br, -*CH*$_2$-CO-) ppm. ^{13}C NMR (100 MHz, D_2O) δ: 174.5 (-NH-*CO*-CH$_2$ from HYPAM core and core-shell link); 71.02 (-*CH*$_2$-O-CH$_3$); 69.7 (-O-*CH*$_2$-*CH*$_2$-O); 60.4 (-O-*CH*$_3$); 58.1 (NH-CO-CH$_2$-*CH*$_2$-O); 51.4-53.6 (N-*CH*$_2$-*CH*$_2$-N and CONH-*CH*$_2$-*CH*$_2$-N); 52.4, 49.2-50.3 (N-*CH*$_2$-CH$_2$-CO); 37.1 (CO-NH-*CH*$_2$- CH$_2$-O) ppm. IR (KBr): ν(cm^{-1}) = 1107, 1539, 1644, 1733, 3428. HYPAM-C$_{18}$-PEG: ^{1}H NMR (400MHz, $CDCl_3$) δ: 4.18 (t, -COO-*CH*$_2$); 3.82-3.40 (br , -O-*CH*$_2$-*CH*$_2$-O- from mPEG_); 3.35 (s, -O-*CH*$_3$); 3.21 (br, -CO-NH-*CH*$_2$-); 2.69 (br, CO-NH-CH$_2$-*CH*$_2$-N- from NHCO-CH$_2$-*CH*$_2$-N- from HYPAM); 2.52 (br, -N-*CH*$_2$-*CH*$_2$-N- and -NH-*CH*$_2$-*CH*$_2$-NH- from HYPAM); 2.30 (t, -*CH*$_2$-COO-); 2.19 (br, NHCO*CH*$_2$); 1.58 (br, NHCO-CH$_2$-*CH*$_2$-(CH$_2$)$_{12}$-*CH*$_2$-CH$_2$-COO); 1.21 (m, NHCO-CH$_2$-CH$_2$-(*CH*$_2$)$_{12}$-CH$_2$-CH$_2$-COO-) ppm. ^{13}C NMR (100 MHz, $CDCl_3$) δ: 174.1 (-NH-*CO*-CH$_2$ from HYPAM core and core-shell link); 173.7 (-CH$_2$-*COO*-); 71.9 (-*CH*$_2$-O-CH$_3$); 70.5 (-O-*CH*$_2$-*CH*$_2$-O); 69.1 (-COO-CH$_2$-*CH*$_2$-); 63.3 (-COO-*CH*$_2$); 58.9 (-O-*CH*$_3$); 53.4 – 55.1 (N-*CH*$_2$-*CH*$_2$-N); 51.1-52.4

(CONH-CH_2-CH_2-N); 49.4-50.6 (N-CH_2-CH_2-CO); 37.6 (-CO-NH-CH_2-CH_2-N-); 36.4 (CO-NH-CH_2- from the core-shell link); 34.1 (NH-CO-CH_2); 28.8-30.9 (NHCO-CH_2-CH_2-$(CH_2)_{12}$-CH_2-CH_2-COO-); 25.9 (-NH-CO-CH_2-CH_2-); 24.8 (-CH_2-CH_2-COO-) ppm. IR (KBr): ν(cm^{-1}) = 1032, 1530, 1644, 3280.

B.3. Methods.

Gd^{3+}/HyPAM interactions. The interactions between the hyperbranched structure and the gadolinium ions were assessed by NMR. In order to limit relaxation phenomenon promoted by the presence of free gadolinium ions, a substoichiometric amount Gd^{3+} relative to polymer capacity was used for these analyses. Moreover in order to obtain a reasonable NMR signal to noise ratio a polymer concentration one hundred times higher than the one used during the synthesis of NPs was required. Stock solutions of HyPAM (2.10^{-4} mol/L) and $Gd(NO_3)_3$ (4.10^{-4} mol/L) were prepared in D_2O. Aliquots of 1 mL were prepared by addition of 500 µL of HyPAM, 0 to 500 µL of $Gd(NO_3)_3$ and completed at 1 mL with D_2O. The pH of each aliquot was then carefully adjusted between 8 and 9 with NaOD (1 mol/L). ^{1}H NMR spectra were recorded on a BrukerARX500 equipped with a cryogenic probe (400 MHz for ^{1}H). Calibration was performed using the chloroform peak at 7.26 ppm for ^{1}H.

$GdPO_4$/polymer nanowire synthesis and analysis. 250µL of $Gd(NO_3)_3$ (1.10^{-3} mol/L) aqueous stock solution were added to 1 mL of various polymer concentrations (from 0 to 8 µM) in water and constitute the precursor n°1. 250 µL of NaH_2PO_4 (1.10^{-3} mol/L) diluted in 1.25 mL of water constitute the precursor n°2. The pH of precursor 1 was adjusted to pH 8-9 with NaOH (0.01 M) or HCl (0.01 M). Precursor 2 was then dropwise added to precursor 1, using a syringe pump with a flowrate = 1.6mL/h, (Neolus needle Ø0.8mm) under stirring. A drop of each aliquot was then placed on a formvar carbon-coated copper TEM grid (Ted Pella Inc.) and left to dry under air. The samples were analyzed with a MET Hitachi HT7700 transmission electron microscope operating at 80 kV accelerating voltage. Size-distribution histograms were determined by using magnified TEM images and by measuring a minimum of 200 particles of each sample, using ImageJ software (http://imagej.nih.gov/ij/). The size distributions observed were analyzed in terms of Gaussian statistics (wc (σ)).

Selected area electron diffraction (SAED) characterization. SAED patterns were obtained on a JEOL-2010F transmission electron microscope to determine the composition of the $GdPO_4$ NPs and crystallographic parameters.

Relaxivity measurements. All MR relaxation time measurements were carried out at 1.4 T on a Minispec mq60 TD-NMR contrast agent analyzer (Bruker Optics, Billerica, MA, USA) at a constant temperature of 37 °C. T_1 relaxation times were measured using an inversion recovery pulse sequence (t_1_ir_mb); T_2 relaxation times were measured using a Carr–Purcell–Meiboom–Gill pulse sequence (t_2_cp_mb). In order to avoid the presence of residual Gd^{3+} free ions, solutions were dialyzed prior to relaxivity measurements.

The Gd-ion content of the $GdPO_4$ NPs was evaluated using a Perkin Elmer Optima 3200 RL inductively coupled plasma atomic emission spectrometer (ICP-AES). Nitric acid was added to complete digest the $GdPO_4$ NPs and measurements were performed at a concentration near 25 ppm.

Determination of hydrodynamic diameter. Dynamic light scattering experiments (DLS) were performed using a Zetasizer Nano-ZS (Malvern Instruments, Ltd, UK) with integrated 4 mW He-Ne laser, λ = 633 nm. DLS analysis was used to extract Zaverage values, derived count rate, intensity and number average distributions for each studied nano-object sample. Zaverage was obtained from five different runs of the number plot. Standard deviations were evaluated from the diameter distribution. The correlation function was analyzed via the general purpose method (NNLS) to obtain the distribution of diffusion coefficients of the solutes. Then, the size of the particle may be estimated from D after making assumption on the shape of the object. In the simple case of spherical particles, one will use the Stokes-Einstein equation. For anisotropic objects, the single exponential decay of the auto-correlation function is still observed for objects typically less than 150 nm. For such particles, various models have been developed to estimate a geometrical parameter of the particles (generally the length assuming a particular thickness over length ratio) from the translational diffusion. For longer objects, the auto-correlation functions are no more a single exponential decay and are influenced by both the translational and rotational diffusion coefficients. Here the hydrodynamic diameter given correspond to the one obtained with Stoke Einstein model. Therefore these values should be taken only as indicative ones for NPs with strong anisotropic shape (see also supporting information for further discussions).

NaCl Stability study. 100 µL of NaCl (0.02 M, 0.2 M and 2 M) stock solutions were added to 100 µL of $GdPO_4$ nanowires aliquots synthesized with HyPAM, HyPAM-PEG, or HyPAM-C_{18}-PEG (5 µM). These solutions were left 15 days to equilibrate and then analyzed though DLS.

Drug loading capacity. 1 µL of Nile Red (9-diethylamino-5-benzo-α-phenoxazinone) stock solution (1.10^{-3} M in THF) was added to aliquots of $GdPO_4$ NPs synthesized with HyPAM, HyPAM-PEG, or HyPAM-C_{18}-PEG. Aliquots were prepared by diluting 200 µL of 5 µM suspensions of polymers to 1 mL total volume in water. Fluorescence measurements were then performed on a PTI® (Photon Technology International) apparatus with a xenon lamp EIMAC of 175W. The spectrofluorimeter was set with excitation and emission slits of 4 nm. Excitation and emission spectra were recorded with λ_{em}=660 nm and λ_{ex}=590 nm respectively, quartz cells of 10 mm path length and 4 nm slit.

Cytotoxicity measurements. The cytotoxicity of $GdPO_4$/HyPAM and $GdPO_4$/HyPAM-PEG nanoparticles against CCRF-CEM (human T-cell acute lymphoblastic leukemia cell line) cancer cells was evaluated using the trypan blue (Sigma-Aldrich, St. Louis, MO, USA). The cells (100 µL of 4×10^5 cells/mL) were added to each test well on a 96-well plate followed by 10 µL of $GdPO_4$/HyPAM or $GdPO_4$/HyPAM-PEG at different concentrations. The resultant cell mixture was incubated at 37°C under a 5% CO2 atmosphere for 24 h. After incubation, 10 µL of the cell mixture was taken from each test well and mixed with 10 µL of 0.4% trypan blue solution. Then fill the hemocytometer chamber with 10 µL mixture and incubate the hemocytometer and cells for 1.5 minutes at room temperature, following by counting cells under microscope. Non-viable cells will be stained by trypan blue, whereas viable cells will be unstained. In addition, bright field images of the trypan blue treated CEM cells were recorded using a confocal laser scanning microscope (Olympus FV 500-IX81).

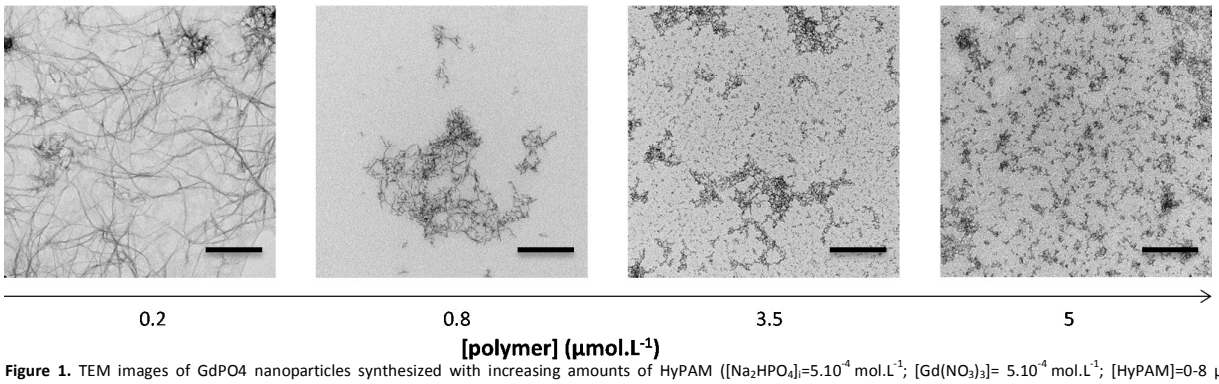

Figure 1. TEM images of GdPO4 nanoparticles synthesized with increasing amounts of HyPAM ($[Na_2HPO_4]_i$=5.10^{-4} mol.L^{-1}; $[Gd(NO_3)_3]$= 5.10^{-4} mol.L^{-1}; [HyPAM]=0-8 µmol.L^{-1} ; $pH_{adjusted}$ = 8-9) , before dialysis, scale bars = 200nm (see enlargement of TEM picture in Figure S5A and S5C).

C. Results and discussion

The synthesis of the hyperbranched polymer core (noted HyPAM) with a similar structure to PAMAM dendrimers was based on the reaction of a hexaester with a trisamine. This method has the advantage to lead to the hyperbranched structure in a single step and can be carried out in large quantities. Its main drawback is to yield polymers with broad molecular weight distributions. The molecular weight of the polymers was easily adjusted by changing the ratio between the triamine and the hexaester. Molar ratios close to 10:1 led to polymers with molecular weight close to those of 4th generation PAMAM. The HyPAM core was then functionalized with linear hydrophilic or amphiphilic building blocks formed by alkyl diacids (C_0 or C_{18}) connected to monomethyl poly(ethylene glycol) ($mPEG_{750}$: PEG with 14 glycol units on average). The attachment of the single or double shell was carried out according to an already published procedure (Figure S1A in ESI).[32] Primary amino groups were functionalized above 90% as demonstrated by ^{1}H NMR (Figure S1B in ESI). The molecular weight of the HYPAM core was evaluated by size exclusion chromatography in a carbonate buffer at a pH of 10 as previously described.[32]An average molecular weight of 13000 g/mol was estimated with a dispersity of 1.4.

Grafting of the single shell induced an increase of molecular weight compatible with the expected theoretical value if estimating 90% of primary terminal amino groups are modified (54000 g/mol). In the case of hyperbranched polymers with a double shell structure, such analysis could not be properly performed, as aggregation phenomenon occurring in water induced a strong overestimation of the molecular weight. However, NMR analysis indicating 90% amine functionalization leads to a molecular weight estimate of 69000 g/mol.

Gadolinium nanoparticles were synthesized under mild conditions by adding an aqueous solution of NaH_2PO_4 (1.10^{-3} M) dropwise onto an aqueous solution of $Gd(NO_3)_3$ (1.10^{-3} M) containing various concentrations of hyperbranched HyPAM-based polymers (see further details in details in experimental section). Similar hyperbranched structures have previously demonstrated higher efficiency relative to their linear counterparts as stabilizers in the synthesis of gold NPs.[34] SAED pattern of $GdPO_4$ NPs (see Figure S2 in ESI) highlights amorphous nanowires. The electron diffraction pattern confirms the formation of $GdPO_4$, the normal crystallographic phase formed out of water, although the exact extent of hydration is not determined.[17] Whereas large nanowires with low colloidal stability were obtained in the absence of HyPAM, the addition of polymer enables formation of stable colloidal solutions of the gadolinium phosphate NPs. Moreover, as illustrated with TEM images in Figure 1 (and Figure S4C in Supporting information), low polymer concentration leads to nanowires but the $GdPO_4$ NPs morphology becomes isotropic with smaller average size at higher polymer concentration. The same trend is observed independent of the functionalization of the hyperbranched core (Figure 2). Therefore the average length of the nanowires can be adjusted by changing the polymer concentration (Figure 2). More polymer leads to a decrease of the average nanowire length from 120±39 nm to 6±2 nm, with nearly isotropic NPs forming at the higher polymer concentration (above 3.5 µmol.L^{-1}). Size control likely results from two effects. Firstly, ^{1}H NMR evidenced a shift and widening of the tertiary amine of vicinal proton upon adding Gd^{3+} to the HyPAM polymers (see Figure S3 in supplementary information), indicating interactions between the HyPAM tertiary amines and Gd^{3+} prior to the addition of sodium phosphate. Secondly, HyPAM can interact with the gadolinium phosphate surface, stabilizing the NPs, as suggested by their higher colloidal stability in the presence of the polymers. Both factors contribute to control over the nucleation and growth processes upon the addition of phosphate.

This polymer-mediated synthesis is the first reported for gadolinium phosphate NPs, affording size control down to 5 nm under aqueous and room temperature conditions. Compared to previous published results, which produced nanorods with lengths above 20 nm, this is a significant achievement towards the synthesis of small $GdPO_4$ NPs.[17-25] Moreover different length nanowires can be assessed and stabilized within the same environment, allowing systematic analyses of size effects.

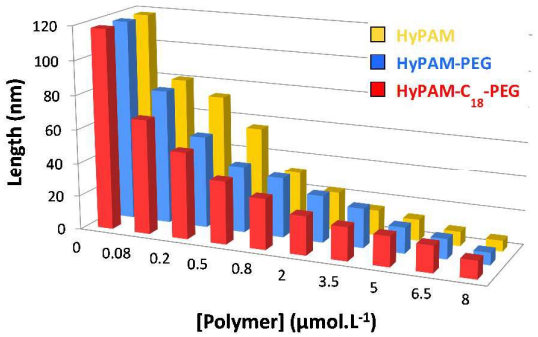

Figure 2. Average lengths of GdPO4 NPs determined from TEM analysis, versus increase concentration of HyPAM, HyPAM-PEG, and HyPAM-C_{18}-PEG (standard deviation relative to length were given in supporting information in Figure S3 and S4).

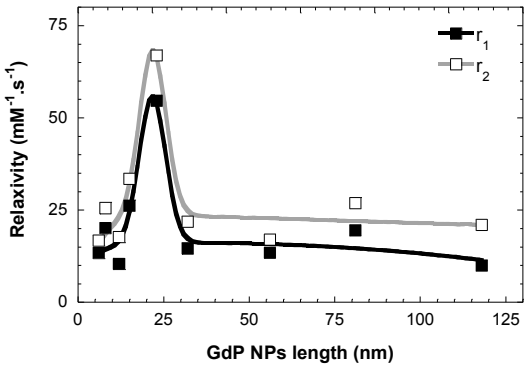

Figure 3. GdPO4/HyPAM size dependence on r1 and r2 relaxivities (1.4 T). Particle lengths were determined before dialysis. Lines are guides to the eye. Standard deviation relative to both length and relaxivity were given in supporting information in Figure S4.

Transversal and longitudinal relaxation times T_1 and T_2 were recorded to assess any size dependence effect (Figure 3). Dialysis to remove any free Gd^{3+} and ICP analysis of Gd content were performed on the samples before relaxivity measurements (see experimental section and supplementary information Figure S4). In Figure 3, a clear dependence of r_1 and r_2 on nanowire length is demonstrated. Moreover the plot indicates an optimum particle size for maximizing relaxivity, similar to the trends reported by Park *et al*. for Gd_2O_3 nanoparticles.[10] For the hybrid $GdPO_4$/HyPAM nanowires, the optimal length was found to be 23±11 nm with exceptionally high relaxivity values of r_1=55±9 $mM^{-1}{\cdot}s^{-1}$ and r_2=67±11 $mM^{-1}{\cdot}s^{-1}$ ([HyPAM]=3.5 µmol/L). To assure the result is intrinsic to the particle hybrids and not the result of trace Gd^{3+} ions still strongly bound to the nanohybrids, a large excess of phosphate was added. After dialysis, no significant modification of NPs size or relaxivity was observed.

These values are higher than those found for molecular T_1 agents and are higher than most gadolinium based particles explored to date. For example, Hifumi *et al.* previously reported gadolinium-based hybrid nanoparticles (PGP/dextran-K01) with r_1 and r_2 of 13.9 and 15.0 $mM^{-1}{\cdot}s^{-1}$ (at 1.5 T).[17] Johnson *et al.* has studied relaxivity dependence of $NaGdF_4$ nanoparticles of different sizes, with the smallest size of 2.5 nm showing r_1 of 2.8 $mM^{-1}{\cdot}s^{-1}$.[35] Another example is ultrasmall gadolinium hydrated carbonate nanoparticles, studied by Liang *et al.*,[36] showing high r_1 of 34.8 $mM^{-1}{\cdot}s^{-1}$.

The particle size dependences of r_1 and r_2 show a maximum for the 23 nm particle sample, with lower values of relaxivity for both larger and smaller particles. Similar observations of an optimal particle size have been observed for other particle systems,[10,37] including $NaGdF_4$ and Gd_2O_3, and is attributed to contributing factors influencing relaxivity that have opposite particle size corelations. The first is the availability of Gd^{3+} ions at the surface, as direct chemical exchange of water molecules is the largest contributor to proton relaxation. The surface to volume ratio (S/V) increases as particle size gets smaller, accounting for the most often observed increase in relaxivity as particles become smaller. On the other hand, correlation times and therefore tumbling times are another factor.[2,4,35,38] Tumbling times depend on the medium viscosity and hydrodynamic volume of the particles. If we assume the viscosity does not change for the different particle suspensions, then for a reasonable range of particle sizes, relaxivity should increase with hydrodynamic volume. For this series with the same chemical coating, the apparent hydrodynamic diameter follows the same linear trend as the increase of NP length from ~10 to ~100 nm, allowing us to consider the NP length as the key parameter. These opposing contributions of surface area and hydrodynamic volume are then expected to give rise to an optimum particle size for any set of conditions, as observed in Figure 3. It is important to realize that correlation times will be affected by other parameters, also, such as medium viscosity and applied magnetic field strength, so any 'optimum' particle size will depend on the application. Furthermore, since the tumbing time depends on the hydrodynamic volume of the composite polymer-particle object, the polymer mediated preparation affords the potential for tuning the response through synthetic variation of both the inorganic particle size and the thickness of the polymer coating.

The hyperbranched polymer mediated synthesis of $GdPO_4$ NPs was extended to the functionalized core-shell HyPAM analogues, HyPAM-PEG and HyPAM-C_{18}-PEG, in order to confer additional properties such as biocompatibility, additional colloidal stability and drug-loading capacity. Similar size control was achieved with these other hyperbranched polymers, as confirmed by TEM analyses in Figure S4 in the ESI. As expected, coating the nanoparticles with these PEG derivatives shifts zeta potential values close to zero, compared to ζ = +28±4 mV for the HyPAM-coated particles resulting from protonation of the amine functions at pH values close to 7.

The stability of colloidal suspensions of the polymer stabilized gadolinium phosphate hybrids was followed with dynamic light scattering, measuring the average hydrodynamic radius under different conditions of added salt, Figure 4. Before the addition of salt, even after filtration, correlograms for HYPAM-PEG and HYPAM-C18-PEG present small bumps at high correlation times (see Figure S6B). They correspond to the formation of aggregates in solution. Their existence can be ascribed to the tendency of those polymers to form agglomerates as previously demonstrated by R. Haag et al..[33] Moreover their presence hampered the accurate determination of hydrodynamic diameter of corresponding particles and explained differences observed between number and intensity weighted values (see Table 1). Whereas $GdPO_4$ NPs coated by HyPAM alone aggregate upon addition of NaCl, the PEG functionalized core-shell polymers ensure high stability of the polymer-particle hybrids against ionic strength, up to 1 M NaCl (see Figure S6 in ESI). In the case of HYPAM-C18-PEG, there was also no evidence of destabilization in the presence of albumin serum. The high affinity of Gd^{3+} ions for phosphate prevents any significant leaching of ions in these conditions. The successful stabilization of the $GdPO_4$ nanowires by the hyperbranched polymers is in line with studies of other hybrid organic/inorganic systems[28,29,39,40]. Furthermore, other examples have shown that pegylated hybrid systems can be dried and easily redispersed in water or organic solvents compatible with the PEG moieties[30,32], a property that could be exploited for storage or transport of these potential contrast agents.

The polymer-particle hybrids can impart additional functions beyond solubility and colloidal stability. For example, the hydrophobic C_{18} layer of core-double shell HyPAM-C_{18}-PEG colloids has also been exploited for it drug loading capacity[31]. To highlight the possibility of this added function, the well-known polarity probe Nile Red[41–43] was added as a surrogate for a hydrophobic drug and the resulting fluorescence intensities were recorded to assess the potential for molecule uptake (see Figure S7 in ESI). As expected,

the $GdPO_4$/HyPAM and HyPAM-PEG polymer-particle hybrids do not exhibit any shift of their maximum emission wavelength compared to water or $GdPO_4$ controls as would be indicative of a change in environment of the Nile red, and thus do not possess any potential as drug carriers. On the other hand, the $GdPO_4$/HyPAM-C_{18}-PEG systems possess an apolar layer in which the Nile Red becomes localized, resulting in a shifted emission wavelength corresponding to a dielectric constant of about ε = 30, illustrating the potential of this hybrid system to act as drug carrier combined with imaging probe.

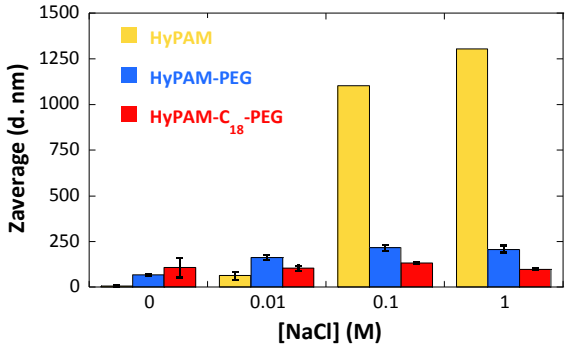

Figure 4. DLS measurements of the GdPO4/hyperbranched polymers (5 µmol/L) upon NaCl addition (0, 0.01, 0.1, 1 mol.L^{-1}); Standard deviations: $\sigma_{HyPAM(0,1M)=}$ 490 nm ; $\sigma_{HyPAM(1M)=}$ 940 nm.

Lastly, r_1 and r_2 relaxivity measurements were performed for the $GdPO_4$ particles stabilized with the PEG-containing hyperbranched polymers. By using the same concentration of polymer, NPs with similar size can be compared (Figure 1), differing only in the nature of the outer shell of the polymer-particle hybrid. Comparisons of the $GdPO_4$ relaxivities for the different particles are gathered in Table 1. The apparent hydrodynamic diameter and NP length were not significantly different for the three studied systems, allowing the influence of the chemical coating to be compared.

Table 1. Relaxivity comparison of $GdPO_4$ coated with HYPAM and functionalized HYPAM polymers (field 1.4 T, [Polymer]=5 µmol.L^{-1}).

	HyPAM	HyPAM-PEG	HyPAM-C_{18}-PEG
$r_{1\ (mM^{-1}.s^{-1})}$	26.2 ±0.3	23.8 ±0.8	13.9 ±0.1
$r_{2\ (mM^{-1}.s^{-1})}$	33.5 ±0.3	36.8 ±1.2	17.2 ±0.2
r_2/r_1	1.3	1.5	1.2
Length $_{(nm)}$	15 ±7	15 ±5	18 ±10
D_h [a]	47±17(66%) (28 ± 8)	56±15 (61%) 30 ± 6	44 ± 10 (42%) 25 ± 5

[a] D_h : hydrodynamic diameter obtained from intensity-weighted size distribution (and number-weighted size distribution). Differences between those two values illustrates the presence of aggregates in solution that strongly impact intensity-weighted values (see complete size distribution in Figure S6A and discussion in supporting information).

The $GdPO_4$ nanowires stabilized by HyPAM and HyPAM-PEG have hydrophilic coatings and therefore exhibit similar r_1 and r_2 values, due to the similarly hydrated environment around the inorganic particle that these two coatings provide. In contrast, the HyPAM-C_{18}-PEG stabilized $GdPO_4$ nanoparticles exhibit lower r_1 and r_2 values, most likely as a result of the hydrophobic C_{18} layer of the hyperbranched structure, which reduces the diffusion of water molecules between the particle surface and the bulk solvent. Nevertheless, the relaxivities of the HyPAM-C_{18}-PEG stabilized particles are still quite reasonable, even if they should be taken, at this step, as indicative values. Indeed their accurate determination is still hampered by the presence of a small fraction of aggregates in solution. Cytotoxicity tests enable evaluation of the efficiency of the PEG shell to render those nanoparticles suitable for biological assays. With $GdPO_4$/HyPAM nanoparticles, decreasing viability of CEM cells was recorded with high hybrid nanoparticle concentrations (Figure 5a and 5d). As already observed in the case of PAMAM structures,[44] this result should be related to the cytotoxicity of the amine functions of the HyPAM polymers. On the contrary, $GdPO_4$/ HyPAM-PEG or HYPAM-C_{18}-PEG shows no toxicity to CEM cells with concentration up to 38.4 µmol L^{-1} (Figure 5b, 5e and Figure S8 in supporting information), confirming the potential for use of the $GdPO_4$ covered by HyPAM-PEG as clinical MRI contrast agents.

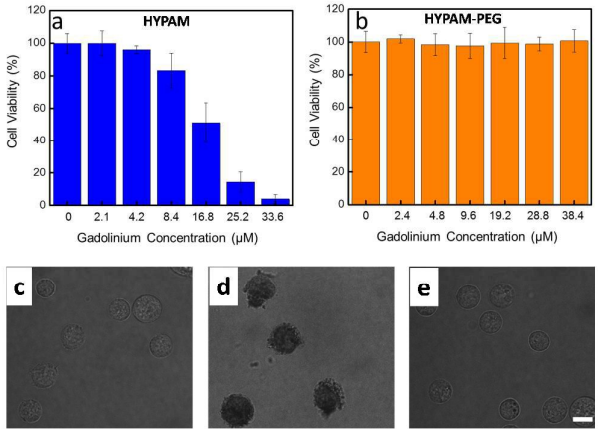

Figure 5. Cell viability of CEM cells in presence of (a) GdPO4/HyPAM and (b) $GdPO_4$/HyPAM-PEG nanoparticles at different concentrations. Bright field images of CEM cells incu-bated (a) without nanoparticles; (b) with GdPO4/HyPAM (33.6 µM); (c) with $GdPO_4$/HyPAM-PEG (38.4 µM). All the samples are imaged after trypan blue staining. Scale bar 10 µm.

Conclusions

Hyperbranched polymers and functionalized core-shell polymers based on the polyamidoamine HyPAM were used to govern the synthesis of size-controled $GdPO_4$ nanowires in aqueous solutions at room temperature. The $GdPO_4$ nanowires were obtained in a range of 120±39 nm down to 6±2 nm with micromolar concentrations of the HyPAMs. Relaxivity measurements of the HYPAM-coated particles over the range of $GdPO_4$ particle sizes revealed an optimal length at ca. 23±11 nm for which promising r_1 and r_2 values were obtained (r_1= 55±9 $mM^{-1}.s^{-1}$; r_2= 67±11 $mM^{-1}.s^{-1}$). The functionalized core-shell polymers HyPAM-PEG and HyPAM-C_{18}-PEG were then used to form similar polymer-particle hybrids in order to improve stability, in vitro toxicity and potentially permit payload loading. These promising properties still necessitate assessing the effectiveness and viability of these hybrid NPs as MRI contrast agents under *in vivo* conditions. Nevertheless, the rather facile synthetic method presented here could also be easily applied

to other families of polymers, and studies are under way to explore the scope of these approaches.

Acknowledgements

The authors thank the "Région Midi-Pyrénées" for the Chair of Excellency "Pierre de Fermat" allocated to D.R.T. Partial funding was also provided by the US National Science Foundation Division of Chemistry under grant no. CHE-0957155, co-funded by the MPS/CHE and the Office of International Science and Engineering (DRT). This work was financially supported by the ANR-DFG pro-gram (ANR-11-INTB-1004, "Dendrion-Bio").

Notes and references

1 H. B. Na, I. C. Song and T. Hyeon, *Adv. Mater.,* 2009, **21**, 2133.
2 A. J. L. Villaraza, A. Bumb and M. W. Brechbiel, C*hem. Rev.,* 2010, **110**, 2921.
3 P. Caravan, J. J. Ellison, T. J. McMurry and R.B. Lauffer, *Chem. Rev.,* 1999, **99**, 2293.
4 P. Caravan, *Chem. Soc. Rev.,* 2006, **35**, 512.
5 S. Laurent, D. Forge, M. Port, A. Roch, C. Robic, L. Vander Elst and R. N. Muller, *Chem. Rev.,* 2008, **108**, 2064.
6. T. Lam, P. Pouliot, P. K. Avti, F. Lesage and A. K. Kakkar, *Adv. Colloid Interface Sci.,* 2013, **199-200**, 95.
7 Y. Cheng, R. Morshed, B. Auffinger, A. L. Tobias and M. S. Lesniak, *Adv. Drug Deliv. Rev.,* 2014, **66**, 42.
8 Z. Cheng, Y. Dai, X. Kang, C. Li, S. Huang, H. Lian, Z. Hou, P. Ma and J. Lin, *Biomaterials,* 2014, **35**, 6359.
9 J.-L. Bridot, A.-C. Faure, S. Laurent, C. Rivière, C. Billotey, B. Hiba, M. Janier, V. Josserand, J.-L. Coll, L. Vander Elst, R. Muller, S. Roux, P. Perriat and O. Tillement, *J. Am. Chem. Soc.,* 2007, **129**, 5076.
10 J. Y. Park, M. J. Baek, E.S. Choi, S. Woo, J.H. Kim, T.J. Kim, J. C. Jung, S. Chae, Y. Chang and G. H. Lee, *ACS Nano,* 2009, **3**, 3663.
11 G. K. Das, B. C. Heng, S.-C. Ng, T. White, J. S. C. Loo, L. D'Silva, P. Padmanabhan, K. K. Bhakoo, S. T. Selvan and T. T. Y. Tan, *Langmuir*, 2010, **26**, 8959.
12 L. Faucher, M. Tremblay, J. Lagueux, Y. Gossuin and M.-A. Fortin, *ACS Appl. Mater. Interfaces,* 2012, **4**, 4506.
13 F. Evanics, P.R. Diamente, F. C. J. M. Veggel, G. J. Van; Stanisz and R. S. Prosser, *Chem. Mater.,* 2006, **18**, 2499.
14 J. Xu, S. Gai, P. Ma, Y. Dai, G.; Yang, F. He and P. Yang, *J. Mater. Chem. B,* 2014, **2**, 1791.
15 P. Lessing and A. W. Erickson, *J. Eur. Ceram. Soc.,* 2003, *23*, 3049.
16 Y.-P. Fang, A.-W. Xu, R.-Q. Song, H.-X. Zhang, L.-P. You, J. C. Yu, H.-Q. Liu, *J. Am. Chem. Soc.,* 2003, **125**, 16025.
17 H. Hifumi, S. Yamaoka, A. Tanimoto, D. Citterio and K. Suzuki, *J. Am. Chem. Soc.,* 2006, **128**, 15090.
18 H.Hifumi, S. Yamaoka, A. Tanimoto, T. Akatsu, Y. Shindo, A. Honda, D. Citterio, K. Oka, S. Kuribayashi and K. Suzuki, J. *Mater. Chem.,* 2009, **19**, 6393.
19 W. Ren, G. Tian, L. Zhou, W. Yin, L. Yan, S. Jin, Y. Zu, S. Li, Z. Gu and Y. Zhao, *Nanoscale,* 2012, **4**, 3754.
20 M. F. Dumont, C. Baligand, Y. Li, E. S. Knowles, M. W. Meisel, G. A. Walter and D. R. Talham, *Bioconjug. Chem.,* 2012, **23**, 951.
21 S. Rodriguez-Liviano, A. I. Becerro, D. Alcántara, V. Grazú, J. M. de la Fuente and M. Ocaña, *Inorg. Chem.,* 2013, **52**, 647.
22 X. Liu and R. H. Byrne, *Geochim. Cosmochim. Acta,* 1997, **61**, 1625.
23 R. A. Laudise and A. A. Ballman, *J. Am. Chem. Soc.,* 1958, **80**, 2655.
24 Y. Hikichi, K. Hukuo and J. Shiokawa, *Bull. Chem. Soc. Jpn.,* 1978, **51**, 3645.
25 Q. Du, Z. Huang, Z. Wu, X. Meng, G. Yin, F. Gao and L. Wang *Dalton Trans.* 2015, **44**, 3934
26 R. Li, Z. Ji, C. H. Chang, D. R. Dunphy, X. Cai, H. Meng, H. Zhang, B. Sun, X. Wang, J. Dong, S. Lin, M. Wang, Y.-P. Liao, C. J. Brinker, A. Nel and T. Xia *ACS Nano*, 2014, **8**, 1771.
27 N. Pérignon, A. F. Mingotaud, J.-D. Marty, I. Rico-lattes and C. Mingotaud, *Chem. Mater.,* 2004, **16**, 4856.
28 N. Pérignon, R. Haag, J.-D. Marty, R. Thomann, N. Lauth-de Viguerie and C. Mingotaud, *Macromolecules,* 2005, **38**, 8308.
29 N. Pérignon, J.-D. Marty, M. Dumont, I. Rico-lattes and C. Mingotaud, *Macromolecules,* 2007, **10**, 3034.
30 J. Keilitz, M. R. Radowski, J.-D. Marty, R. Haag, F. Gauffre and C. Mingotaud, *Chem. Mater.,* 2008, **20**, 2005.
31 M. Beija, R. Salvayre, N. Lauth-de Viguerie and J.-D. Marty, *Trends Biotechnol.,* 2012, **30**, 485.
32 S. Saliba, C. Valverde Serrano, J. Keilitz, M. L. Kahn, C. Mingotaud, R. Haag and J.-D. Marty, *Chem. Mater.,* 2010, **22**, 6301.
33 M. R. Radowski, A. Shukla, H. von Berlepsch, C. Böttcher, G. Pickaert, H. Rehage and R. Haag, *Angew. Chem. Int. Ed. Engl.,* 2007, **46**, 1265.
34 H. H. Nguyen, A. Brûlet, D. Goudounèche, P. Saint-Aguet, N. Lauth-de Viguerie and J.-D. Marty, *Polym. Chem.*, 2015, 6, 5838-5850.
35 N. J. J. Johnson, W. Oakden, G. J. Stanisz, R. S. Prosser, R. S.; F. C. J. M. Van Veggel, *Chem. Mater.,* 2011, **23**, 3714.
36 G. Liang, L. Cao, H. Chen, Z. Zhang, S. Zhang, S. Yu, X. Shen and J. Kong, *J. Mater. Chem. B,* 2013, **1**, 629.
37 Y. Hou, R. Qiao, F. Fang, X. Wang, C. Dong, K. Liu, C. Liu, Z. Liu, H. Lei, F. Wang and M. Gao, *ACS Nano,* 2013, **7**, 330.
38 E. Wiener, M. W. Brechbiel, H. Brothers, R. L. Magin, O. A. Gansow, D. .A. Tomalia and P. C. Lauterbur, *Magn. Reson. Med.,* 1994, **31**, 1.
39 H. Ye, R. W. J. Scott and R. M. Crooks, *Langmuir,* 2004, *20*, 2915.
40 J.-D. Marty, E. Martinez-Aripe, A.-F. Mingotaud and C. Mingotaud, *J. Colloid Interface Sci.,* 2008, **326**, 51.
41 P. Greenspan and S. D. Fowler, *J. Lipid Res.,* 1985, **26**, 781.
42 D. L. Sackett and J. Wolff, *Anal. Biochem.,* 1987, **167**, 228.
43 T. Behnke,C. Würth, K. Hoffmann, M. Hübner, U. Panne and U. Resch-Genger, *J. Fluoresc.*. 2011, **21**, 937.
44 N. Tag, P. K. Mutlu and U. Gunduz, *J. Nanoparticle Res.*, 2014, **16**, 2342.